A Synthetic Recursive "+1" Pathway for Carbon Chain Elongation

Ryan J. Marcheschi[†,#], **Han Li**[‡,#], **Kechun Zhang**[†,#], **Elizabeth L. Noey**[§], **Seonah Kim**[§], **Asha Chaubey**[§,‖], **K. N. Houk**[§], and **James C. Liao**[*,†,§,⊥]

[†]Department of Chemical and Biomolecular Engineering, University of California, Los Angeles, California 90095, United States

[‡]Molecular Biology Institute, University of California, Los Angeles, California 90095, United States

[§]Department of Chemistry and Biochemistry, University of California, Los Angeles, California 90095, United States

[⊥]Institute for Genomics and Proteomics, University of California, Los Angeles, California 90095, United States

[‖]Indian Institute of Integrative Medicine (CSIR), Jammu 180001, India

Abstract

Nature uses four methods of carbon chain elongation for the production of 2-ketoacids, fatty acids, polyketides, and isoprenoids. Using a combination of quantum mechanical (QM) modeling, protein–substrate modeling, and protein and metabolic engineering, we have engineered the enzymes involved in leucine biosynthesis for use as a synthetic "+1" recursive metabolic pathway to extend the carbon chain of 2-ketoacids. This modified pathway preferentially selects longer-chain substrates for catalysis, as compared to the non-recursive natural pathway, and can recursively catalyze five elongation cycles to synthesize bulk chemicals, such as 1-heptanol, 1-octanol, and phenylpropanol directly from glucose. The "+1" chemistry is a valuable metabolic tool in addition to the "+5" chemistry and "+2" chemistry for the biosynthesis of isoprenoids, fatty acids, or polyketides.

Engineering microorganisms to synthesize bioderived molecules from renewable carbon sources has drawn increasing attention in recent years. Biological synthesis is an important step toward sustainable production of fuels[1–4] or chemicals[5–7] to replace petroleum-based approaches. However, even though nature has a diverse set of enzymes and metabolic pathways to generate primary or secondary metabolites,[8] many useful chemicals are not accessible through natural biosynthetic pathways. For example, while more than 1 billion pounds of 1-pentanol, 1-hexanol, 1-heptanol, and 1-octanol are produced annually by chemical synthesis,[9] no metabolic pathways have been identified to make these alcohols. To

broaden the applications of biosynthesis, it is necessary to expand the metabolite repertoire of living systems to cover more industrial chemicals. We previously engineered a biosynthetic pathway to elongate the carbon chain of 2-keto-3-methylvalerate and produced a branched six-carbon alcohol.[10] In this study, using a combination of QM modeling, protein–substrate complex modeling, structure-based protein engineering, and metabolic engineering, we expand the substrate range of this "+1" pathway from branched-chain ketoacids to linear-chain and even aromatic-chain 2-ketoacids.

The natural role of our target "+1" pathway is for the bio-synthesis of ketoisocaproate.[11] The catalytic cycle (Figure 1a) begins with the condensation of acetyl-CoA to ketoisovalerate (KIV) catalyzed by 2-isopropylmalate synthase (LeuA).[12] Then, isopropylmalate isomerase complex (LeuCD) catalyzes the conversion of (2S)-2-isopropylmalate (**1**) to (2R,3S)-3-isopropylmalate (**2**) after dehydration and trans-rehydration.[13] Finally, isopropylmalate dehydrogenase (LeuB) catalyzes the oxidation of **3** to (2S)-2-isopropyl-3-oxosuccinate (**4**) and decarboxylation of **4** to ketoisocaproate.[14] The net effect of one catalytic cycle is the addition of one carbon unit to the input substrate. If the selectivity of the "+1" pathway is altered, it could be a very useful tool for biosynthesis of nonnatural ketoacids with elongated carbon chains and possibly nonnatural alcohols upon enzymatic decarboxylation and reduction (Figure 1b,c). Since LeuA is the first committed enzyme of the elongation pathway and mutating LeuA in *Escherichia coli* (*Ec*LeuA) could change the pathway selectivity on branched-chain substrates,[10] we investigated the effect of modulating the substrate specificity of *Ec*LeuA on linear-chain and aromatic-chain substrates.

RESULTS AND DISCUSSION

Analysis of Potential Use of Long-Chain Substrates by LeuA

To address the feasibility of using LeuA to catalyze recursive elongation of long-chain substrates, we performed QM calculations of the transition state of the carbon–carbon bond-formation step catalyzed by LeuA, modeled as shown (Figure 2). These calculations determined the best conformation and geometry for the transition state for this step and showed how the free energy changes as a function of the R group on the 2-ketoacid. Because this model is simplified compared to the reaction in the protein, the absolute energy barrier is not highly accurate but gives a good indication of how the barrier changes as a function of the R group on the 2-ketoacid.

The conformation of the transition state follows the Felkin–Anh model for nucleophilic attack on a carbonyl.[15,16] The largest substituent on the carbon adjacent to the carbonyl is antiperiplanar to the attacking nucleophile (Figure 2b). This conformation is nearly identical to that of KIV in the *Mycobacterium tuberculosis* LeuA (*Mt*LeuA) crystal structure[17] (Figure 2c) and fits well into the active site of LeuA (Figure 2d). The forming carbon–carbon bond distance is about 2.04 Å for alkyl-chain substrates and varies slightly with substitution.

All alkyl-chain substrates have predicted activation energies of about 9 kcal/mol (Table 1), indicating that increasing chain length or the branched nature of the R group does not change the activation free energy of the reaction. Therefore, there is no intrinsic barrier to the use of long alkyl-chain substrates by LeuA. In addition to alkyl-chain substrates, we also performed calculations for the aromatic substrates phenylpyruvate (PPy) and homophenylpyruvate (HPPy) to examine the potential for their elongation by LeuA. We found that in these cases, as compared to alkyl chains, the activation energy ($\Delta G^{\ddagger}$) is lowered by 2.7 kcal/mol for PPy and by 1.6 kcal/mol for HPPy, indicating that there is also no apparent barrier to the use of these substrates by LeuA. This decreased activation energy

is due to the electron-withdrawing nature of the phenyl ring, which makes the α-keto carbon of the substrate that is the target of nucleophilic attack by acetyl-coA more electrophilic. This observation was confirmed using calculations of p-chlorophenylpyruvate, which had a $\Delta G^{\ddagger}$ of 3.5 kcal/mol.

From these calculations it is clear that the steric effects of the R group do not greatly affect the barrier for this reaction, but the electronics of the substituent are important. Combined, these data suggest that there is no barrier to the recursive elongation of linear-chain substrates or even aromatic substrates as long as they can fit into the enzyme active site and substrate binding pocket and are oriented appropriately with respect to the residues involved in coordination of the metal ion and the substrate (Figure 2d).

Structure-Based Protein Engineering and Modeling of LeuA–Substrate Molecular Complexes

Residues in the substrate-binding pocket of *Ec*LeuA (His97, Ser139, Asn167, Pro169) were identified on the basis of the crystal structure of *Mt*LeuA (PDB 1SR9, corresponding residues are His167, Ser216, Asn250, and Pro252).[17] These residues are located within a radius of 4.5 Å of the γ-methyl group of the bound ketoisovalerate in the structure and likely influence substrate binding (Figure 2d). To increase the size of the substrate-binding pocket, these residues were systematically mutated to smaller amino acids such as alanine or glycine to enlarge the binding pocket of *Ec*LeuA and allow the accommodation of bigger substrates. A series of *Ec*LeuA mutants based on the leucine-feedback-insensitive *G462D* *Ec*LeuA mutant[18] were made, and their binding-pocket volumes were analyzed by CASTp[19] (http://sts.bioengr.uic.edu/castp/index.php) (Table 2). A comparison of the increased active-site volume in the largest of these mutants (50.0 Å^3, 83% increase over the *G462D* mutant) versus the increase in molecular van der Waals volume of the substrates relative to 2-ketobutyrate predicts that the *H97A/S139G/N167G/P169A/G462D* *Ec*LeuA mutant should be accessible to the range of substrates examined by QM modeling (Table 2).

Molecular modeling of the *G462D* *Ec*LeuA and the *H97A/S139G/N167G/P169A* *Ec*LeuA mutants with RosettaDesign[20] was performed to examine this prediction in greater detail. The quantum mechanically optimized conformations of each substrate were used as an input along with either the *G462D* mutant enzyme based on PDB 1SR9 or a mutant enzyme based on 1SR9 containing the *H97A/S139G/N167G/P169A/G462D* mutations. Overall, all models exhibited similar packing scores (Supplementary Table S1), indicating that the conformation of the active site is well-folded and internal to the protein structure, an observation that is confirmed upon analysis of the energy-minimized output structures in comparison to their respective input structures. To prevent substrates from leaving the active site during refinement, a high force constant was applied to keep them in the vicinity of the catalytic residues (His202, His204 in *Ec*LeuA). Modeling results indicate that the KIV, 2-ketobutyrate (C4), and 2-ketovalerate (C5) substrates are well-positioned in the active site of the *G462D* enzyme and have ligand-binding scores of 2.4, 3.3, and 4.1, respectively (Figure 3a, Supplementary Figure S1, Supplementary Table S1). The 2-ketocaproate (C6) substrate shows a potential steric clash with the interior of the active site and has a ligand-binding score of 18.2, while the 2-ketoheptanoate (C7), 2-ketooctanoate (C8), and aromatic substrates have significant steric clashes with the protein, indicated by their high (*i.e.*, > 40) ligand-binding scores (Figure 3a, Supplementary Figure S1, Supplementary Table S1). These observations predict that the *G462D* enzyme will use the KIV, C4, C5, and possibly the C6 substrate and will not use the C7–C8 or aromatic substrates due to their inability to fit well into the active site. Modeling results for the *H97A/S139G/N167G/P169A/G462D* mutant enzyme revealed that the KIV, C4–C7, and aromatic substrates all fit well into the active site and have ligand-binding scores that are all less than 3.5 (Figure 3a, Supplementary Figure S1, Supplementary Table S1), predicting that this mutant enzyme will

be able to use all these substrates. The C8 substrate has a higher ligand-binding score of 27.6 but shows only limited potential steric clashes with the active site (Figure 3a, Supplementary Figure S1, Supplementary Table S1), so its use by the *H97A/S139G/N167G/P169A/G462D* mutant enzyme is possible but not predicted definitively.

In addition to these predictions of enzyme-binding of substrates, the solvent-accessible surface area (SASA) was examined for each substrate in the protein–substrate complexes (Figure 3b) to predict which substrate(s) would be most preferred by the *G462D* and *H97A/ S139G/N167G/P169A/G462D* mutant enzymes. The basis for this predicted substrate selectivity is the hydrophobic effect, where the substrate that is able to exclude the most water from the active site (thus having the least SASA) will be the preferred substrate for the enzyme. For the *G462D* enzyme model, the SASA is smallest for the C4 substrate, whereas for the *H97A/S139G/N167G/P169A/G462D* mutant enzyme the SASA is smallest for the HPPy aromatic substrate, although the C6 substrate has a similarly small SASA (Figure 3b). Additionally, in the protein–substrate complex models, the C4 substrate fits well into the *G462D* enzyme binding pocket and occupies most of the available volume (Figure 3c), as compared to the *H97A/S139G/N167G/P169A/G462D* mutant-enzyme binding pocket where the substrate occupies only a portion of the available volume (Figure 3d). These observations indicate that the C4 substrate may be the preferred substrate for the *G462D* enzyme, whereas either the C6 or the HPPy substrate (or both) will be the preferred substrate(s) for the *H97A/S139G/N167G/P169A/G462D* mutant enzyme. Interestingly, the C6 substrate is approximately 34 Å^3 larger than the C4 substrate (Table 2), correlating well with the gain in solvent-accessible volume in the *H97A/S139G/N167G/P169A/G462D* mutant-protein active site relative to the *G462D* protein active site (50.0 Å^3, Table 2) and strengthening the prediction that the C6 substrate will be preferred by the *H97A/S139G/ N167G/P169A/G462D* mutant enzyme. Also of note, the C7 substrate is approximately 50 Å^3 larger than the C4 substrate (Table 2), an identical volume increase as that of the active site, and it fits well into the *H97A/S139G/N167G/P169A/G462D* mutant-enzyme binding pocket (Figure 3e). This volumetric correlation and protein–substrate complex model predict that the C7 substrate may be used preferentially to the C4, C5, and C8 substrates (although not the C6 substrate) in the *H97A/S139G/N167G/P169A/G462D* mutant enzyme.

Enzyme Kinetics of Feedback-Resistant and Mutant *Ec*LeuA

Enzymatic assays were performed on *G462D Ec*LeuA (feedback-resistant) and the quintuple mutant *H97A/S139G/N167G/P169A/G462D Ec*LeuA to test the QM and molecular modeling predictions and examine substrate range and specificity. *G462D Ec*LeuA is active on the C4, C5, and C6 substrates (Table 3). The enzyme has the highest activity for 2-ketobutyrate, as measured by its catalytic rate constant (k_{cat}). Activity decreases 3-fold toward 2-ketovalerate and 100-fold toward 2-ketocaproate. The most preferred substrate, as measured by catalytic efficiency (k_{cat}/K_m), is 2-ketobutyrate (Table 3). Catalytic efficiency is 1.3-fold lower for 2-ketovalerate and 28-fold lower for 2-ketocaproate as compared to 2-ketobutyrate. There is no detectable activity for *G462D Ec*LeuA toward 2-ketoheptanoate, 2-ketooctanoate, or aromatic substrates (Table 3).

Several differences in specificity were observed for the *H97A/S139G/N167G/P169A/ G462D* mutant *Ec*LeuA. This mutant *Ec*LeuA has a broader substrate range than *G462D Ec*LeuA, and activity is seen for all substrates, as predicted by the QM calculations. Despite having similar activities toward the alkyl-chain C4–C8 substrates with k_{cat} values in the range of 3.27 to 6.51 s^{-1}, the most preferred substrates for the enzyme are 2-ketocaproate and 2-ketoheptanoate (Table 3). The catalytic efficiencies of these substrates are approximately 2-fold higher than that of 2-ketooctanoate and approximately 3-fold higher than for 2-ketobutyrate and 2-ketovalerate. The enzyme has less activity for the aromatic substrates than for the linear substrates, with k_{cat} values of 0.091 and 0.38 s^{-1} for

phenylpyruvate and homophenylpyruvate, respectively, and has similar catalytic efficiencies for both aromatic substrates (0.77 and 0.66, respectively). The lower activity of the quintuple mutant EcLeuA for the aromatic substrates may be due to their deviation from the ideal transition state distance for all other substrates (2.04 ± 0.01 Å versus 2.12 Å and 1.98 Å for PPy and HPPy, respectively, Table 1) as predicted by QM calculations. In the context of the enzyme active site, these deviations may result in the observed decrease in activity for the aromatic substrates.

These kinetic data agree well with the predictions of the QM and RosettaDesign modeling, particularly for the alkyl-chain substrates. As predicted, the preferred substrate for the *G462D* enzyme is C4, and the preferred substrate(s) for the *H97A/S139G/N167G/P169A/ G462D* mutant enzyme are C6/C7. However, the prediction that the aromatic substrate homophenylpyruvate would be the most preferred substrate for the *H97A/S139G/N167G/ P169A/G462D* mutant enzyme was not supported, indicating that other factors, such as deviation from the ideal transition state distance, are involved in the use of the aromatic substrates by this mutant EcLeuA in addition to solvent exclusion by the substrate and the electronic state of its a-keto carbon. Nonetheless, the *H97A/S139G/N167G/P169A/G462D* mutant EcLeuA was capable of using the aromatic substrates, as predicted by the QM calculations, enabling the recursive elongation of aromatic 2-ketoacids.

Metabolic Engineering of *Ec*LeuA-Catalyzed "+1" Recursive Elongation Pathway in *E. coli*

Finally, we examined the activity of the EcLeuA mutants (Table 2) *in vivo*. The series of mutants were individually constructed into an operon composed of six genes in the transcriptional order *leuA* leuB leuC leuD kivd adh6* (Figure 4a) under the control of the PLlacO1 promoter on a high copy plasmid (pZE_LeuABCDKA6). Kivd is a mutant (*F381L/ V461A*) form of 2-ketoacid decarboxylase from *Lactococcus lactis*,[10] and Adh6 is the alcohol dehydrogenase VI from *Saccharomyces cerevisiae*.[21] Introduction of Kivd and Adh6 enables the conversion of 2-ketoacid products into alcohols. The production host is a modified threonine-hyperproduction strain (ATCC98082 Δ*rhtA*) with the deletion of the threonine transporter gene *rhtA*.[22] Overexpression of *thrABC*[10] in a low copy plasmid helps drive the carbon flux toward threonine. Another operon in the transcriptional order *ilvA leuA* was also built on a medium copy plasmid (Figure 4a). IlvA is the *Bacillus subtilis* threonine dehydratase that is active in converting threonine into 2-ketobutyrate.[22] The additional overexpression of *G462D Ec*LeuA in the medium copy plasmid is to provide basal elongation activity for small substrates,[23] which is required for more robust production of alcohols longer than 1-butanol (Table 4). The final production strain has a total of 11 genes overexpressed.

Alcohol products produced during fermentative growth were identified by GC–MS and quantified by GC–FID (Table 4, Supplementary Figure S2). The *G462D Ec*LeuA produced primarily 1-pentanol (955 mg L^{-1}), with small amounts of 1-butanol and 1-hexanol also produced (Table 4). This reflects the *in vitro* enzyme activity, where the C4 and C5 substrates are efficiently used, converting the initial 2-ketobutyrate supplied through the threonine biosynthesis pathway and the action of IlvA into 2-ketovalerate and 2-ketocaproate recursively, with the 2-ketocaproate subsequently decarboxylated and dehydrogenated by Kivd and Adh6, resulting in 1-pentanol formation. The EcLeuA mutants with expanded active-site volumes yielded additional long-chain alcohols. The *S139G/ G462D Ec*LeuA mutant produced 4.8 mg L^{-1} 1-heptanol, an alcohol never before produced directly from glucose, in addition to significant amounts of 1-butanol and 1-pentanol (Table 4). As the volume of the active site was increased by further mutation, the amount of 1-hepanol also increased up to 77 mg L^{-1} for the *S139G/H97A/N167A/G462D Ec*LeuA mutant (Table 4). This is not a perfect correlation, however, as the *S139G/H97A/N167G/ G462D Ec*LeuA mutant produced only 41 mg L^{-1} 1-heptanol (Table 4). The mutant with the

largest active site volume, *H97A/S139G/N167G/P169A/G462D Ec*LeuA, recaptured the trend of increasing long-chain alcohol production and produced 80.2 mg L^{-1} 1-heptanol and even 2.0 mg L^{-1} 1-octanol (Table 4). None of the other mutants were capable of producing 1-octanol (Supplementary Figure S2, Supplementary Figure S3). These results indicate that our engineered *Ec*LeuABCD module can catalyze the recursive elongation of the natural metabolite 2-ketobutyrate over 5 cycles to 2-ketooctanoate (**10**) (Figure 4a). This C9 ketoacid and the other smaller ketoacids produced by recursive elongation were then converted into 1-butanol, 1-pentanol, 1-hexanol, 1-heptanol, and 1-octanol *in vivo* by Kivd and Adh6.[24]

To investigate the applicability of the "+1" pathway to aromatic substrates *in vivo*, we transformed the *leuA*-leuB-leuC-leuD-kivd-adh6* operon encoding *S139G/H97A/N167G/ P169A/G462D Ec*LeuA into the phenylalanine-overproducing *E. coli* strain ATCC31884 (Figure 4b). Remarkably, besides 664.4 mg L^{-1} phenylethanol, 4.1 mg L^{-1} phenylpropanol was identified in the final fermentation mixture (Supplementary Figure S3). Without the quintuple mutant *Ec*LeuA, phenylpropanol was not produced (data not shown). These results demonstrate that the *Ec*LeuABCD "+1" pathway could even elongate aromatic-substrate phenylpyruvate (**12**) into homophenylpyruvate (**13**) (Figure 4b) *in vivo*.

Conclusions

In this study, we have demonstrated the utility of using a combination of QM modeling, protein–substrate complex modeling, structure-based protein engineering, and metabolic engineering to design, analyze, and produce bacterial strains capable of producing 1-octanol, 1-heptanol and phenylpropanol. Prior to this study, the latter two long-chain alcohols had never before been produced directly from glucose in *E. coli*, a process that represents five iterations of the engineered *Ec*LeuABCD pathway. (However, during preparation of this article, 1-hexanol[25] and 1-octanol[26] were produced via a coenzyme A-dependent reverse *β*-oxidation pathway in *E. coli*.) The other enzymes involved in the alcohol production pathway (LeuCD, LeuB, Kivd, and Adh6) have demonstrated remarkable plasticity in enabling production of long-chain and aromatic alcohols despite not being selected and modified for such activity. Indeed, the enzymatic reactions catalyzed by these enzymes may be limiting steps for the continued iteration of carbon-chain elongation in the *Ec*LeuABCD pathway, as *in vitro Ec*LeuA enzyme assays indicate that robust catalytic efficiency is retained even for the C8 substrate, while only a small quantity of 1-octanol is produced *in vivo*. In particular, LeuCD may not be capable of using much larger substrates relative to the native isopropylmalate substrate. This enzyme complex has been studied in *M. jannaschii*[27] and is approximately 35% identical to the *E. coli* LeuCD, as determined by BLAST[28] (www.ncbi.nlm.nih.gov/BLAST). The *M. jannaschii* LeuCD actually had higher activity for smaller substrate analogues of isopropylmalate than for the native substrate itself.[27] Although no larger substrates were analyzed, if this trend continues, substrates such as butylmalate, pentylmalate, and hexylmalate may not be usable by the enzyme, hence limiting the throughput of the "+1" elongation pathway.

LeuB has been studied in both *E. coli*[29,30] and *T. thermophilus*,[31] with differing substrate ranges reported for each organism-specific enzyme, despite being 51% identical.[30] *E. coli* LeuB had similar catalytic activities of 70 s^{-1} and 60 s^{-1} for ethylmalate and isopropylmalate, respectively, but no activity was observed for isobutylmalate and no larger substrates were tested,[29] while *T. thermophilus* LeuB had catalytic activities from approximately 30–49 s^{-1} for the substrates ethylmalate, isopropylmalate, isobutylmalate, and isoamylmalate.[31] These obsevations suggest that LeuB may be substrate-limited in *E. coli* but LeuB enzymes from other organisms may be able to circumvent this potential limitation. We are currently investigating this hypothesis.

Kivd, while not limiting to the process of "+1" chain elongation, may possibly be limiting for alcohol production at the 2-ketoacid decarboxylation step of the pathway (Figure 1). This enzyme has reduced activity on substrates larger than the native ketoisovalerate, with about 23%, 17%, 7%, and 9% relative activities for ketoisocaproate, ketomethylvalerate, ketometylthiobutyrate, and phenylpyruvate, respectively.[32] We have also previously shown that Kivd has about 28% relative activity on ketomethylhexanoate as compared to ketoisovalerate.[10] These data indicate that larger substrates are not used as efficiently as the native substrate. While our mutant Kivd has an enlarged active site that allows for about 110% relative activity on ketomethylhexanoate as compared to ketoisovalerate,[10] its properties for other substrates remain to be determined and are the subject of our current studies.

Adh6, like Kivd, is not limiting to "+1" chain elongation. Further, this enzyme is active on a broad range of substrates with similar activities for aldehydes from pentanal to octanal,[33] so it is not expected to be limiting to alkyl-chain or aromatic alcohol production.

QM modeling of the reaction catalyzed by *Ec*LeuA and molecular modeling of the protein–substrate complex have given insight into the role of steric effects, SASA, and hydrophobicity of the ligand on binding. These models show the strengths and weaknesses of *Ec*LeuA for metabolic engineering and will be expanded upon to reengineer *Ec*LeuA to either attain greater substrate specificity for long-chain 2-ketoacids or accept even more diverse substrates to allow further recursive cycles. Engineering of these enzymes for increased activity on long-chain and aromatic substrates using the methods described here may further advance long-chain alcohol production, as well as the production of an expanded range of nonnatural metabolites, which are useful for a variety of purposes.

In summary, by engineering *Ec*LeuA to be active on aromatic or long-chain aliphatic ketoacids, we turned *Ec*LeuABCD into a flexible biosynthetic pathway for recursive "+1" elongation of the carbon chain of branched-chain,[10] linear-chain, and even aromatic-chain ketoacids. This synthetic elongation pathway is a nice complement to the "+5" and "+2" chemistries existing in nature to produce isoprenoids,[34] polyketides, and fatty acids[35] for the production of industrially and pharmaceutically relevant metabolites. The combination of QM calculations, molecular modeling, and metabolic engineering described in this work has been successful in identifying and modeling enzymes and reactions that can be modified to perform in a recursive manner and may be applied to the investigation and modification of other biosynthetic pathways, such as branched-chain amino acid synthesis and isobutanol production using acetolactate synthase,[1] to produce additional nonnatural metabolites and long-chain biofuels.

METHODS

Vector Construction

Plasmids pZS_thrO, containing the *thrA^{fbr}BC* operon under control of the P_{LlacO1} promoter, and pZE_LeuABCDKA6, containing the *leuA^{fbr}BCD*; *kivd*; *adh6* operon under control of the P_{LlacO1} promoter, were previously constructed.[10] Plasmid pZAlac_ilvA_{BS}leuA, containing the *ilvA* gene from *Bacillus subtilis* and the *leuA^{fbr}* gene from *Escherichia* coli under control of the P_{LlacO1} promoter, was constructed by amplifying the threonine dehydratase gene (*ilvA*) from the genomic DNA of *B. subtilis* using the primer pair IlvAbsaccfwd/IlvAbssalrev.[22] This fragment was digested with Acc65I and SalI. The *leuA^{fbr}* gene was amplified from *E. coli* genomic DNA using the primer pair LeuAsalfwd/LeuAxbarev (sequences available in Supporting Information). This fragment was digested with SalI and XbaI. The fragments were ligated and inserted into pZElac[22] to create plasmid pZElac_ilvA_{BS}_leuA. The replication origin was changed from colE1 to p15A by digesting

pZA31-luc[36] with AvrII and SpeI. The shorter fragment was gel-purified and cloned into pZElac_ilvA$_{BS}$leuA cut with the same enzymes, creating pZAlac_ilvA$_{BS}$_leuA.

Fermentation Procedure

For *n*-alcohol production, the threonine-hyperproduction strain ATCC98082 with *rhtA* knockout[22] was transformed with pZS_thrO, pZAlac_ilvA$_{BS}$leuA, and pZE_LeuABCDKA6 containing various *Ec*LeuA mutations. For aromatic-alcohol production, the phenylalanine-hyperproduction strain ATCC31884 was transformed with pZE_LeuABCDKA6 containing the *H97A/S139G/N167G/P169A/G462D Ec*LeuA mutant. Fermentations for alcohol production were carried out as previously described,[10] with the total incubation time being 48 h.

GC–MS and GC–FID Analysis

Alcohols were subjected to mass analysis and quanitification as previously described.[10] For detection of phenylpropanol and 1-octanol, alcohols were extracted by 0.5 mL of *n*-hexane from 5 mL of fermentation medium. GC oven temperature was initially placed at 85 °C for 2 min. Temperature was increased with a gradient of 45 °C min^{-1} until reaching 118 °C. Then, temperature was increased with a gradient of 0.5 °C min^{-1} until reaching 119 °C, followed by a gradient of 65 °C min^{-1} until reaching 182 °C, which was held for 4 min. Finally, temperature was increased with a gradient of 65 °C min^{-1} until reaching 235 °C and held for 3 min. Representative GC–FID data are available in Supporting Information.

Protein Expression and Purification

Genes encoding *H97A/S139G/N167G/P169A/G462D* LeuA were amplified from plasmid pZE_LeuABCDKA6 and cloned into pQE9 (Qiagen) as previously described[10] to create pQE_hisleuA_GSAGA. The plasmid pQE_hisleuA_GD, containing the *leuA^{fbr}* gene was previously created.[10] Transformation, growth, induction, and purification conditions were performed as previously described.[10]

Enzymatic Assay

Compounds 2-ketoisovalerate, 2-ketobutyrate, 2-ketovalerate, 2-ketocaproate, 2-ketooctanoate, phenylpyruvate, 5,5′-dithio-bis(2-nitrobenzoic acid) (DTNB), and acetyl-CoA were purchased from Sigma-Aldrich. Homophenylpyruvate was purchased from Chembridge Inc. and 2-ketoheptanoate was custom synthesized by AsisChem, Inc. Protein concentration was determined by measuring UV absorbance at 280 nm using an extinction coefficient of 30,020 cm^{-1} M^{-1}. Enzyme was incubated at 30 °C with various ketoacids in 100 mM KCl, 2 mM MgCl$_2$, 100 mM Tris buffer pH 8.0 in a total volume of 50 or 100 μL. Acetyl-CoA was added to 1 mM to start the reactions. After 20 min, reactions were stopped by adding 3 assay volumes of ethanol. Thereafter, 2 assay volumes of 1 mM DTNB in 100 mM Tris buffer, pH 8.0 was added, and the resulting yellow color was measured at 412 nm. All values were baseline-corrected using a blank lacking the respective ketoacids in each assay. A molar extinction coefficient of 13,600 cm^{-1} M^{-1} was used in these calculations.

Quantum Mechanical Calculations

All calculations were performed with Gaussian09[37] with a hybrid density functional (B3LYP) with 6-31G(d) basis set. Optimization and frequency calculations were done in solution using the CPCM model for ethylphenylether, ε = 4.1797. This solvent was chosen for its dielectric constant, which is close to that of the inside of a protein.[38,39] A model for the C–C bond formation step in LeuA was used to determine the activation free energy for this step with a variety of 2-ketoacids. This model includes 1-(methylthio)ethenolate[40] as a model for acetyl-CoA attacking the 2-ketoacids (Figure 2).

Protein Modeling Using RosettaDesign

Initial protein–substrate complex models were made by superimposing geometry-optimized (resembling the transition state for carbon–carbon bond formation) substrates containing various R groups (alkyl or aromatic) onto the ketoisovalerate substrate present in the *Mt*LeuA crystal structure (PDB 1SR9). Amino acid side chains in the vicinity of these superimposed substrates were then reoriented using low energy rotamers to minimize unfavorable steric interactions with the substrates. Full optimization of protein packing and active-site residue conformations was then carried out to generate one energy-minimized protein–substrate model for each substrate examined. The substrate coordinates were held fixed for this first step. Next, mutations were made in the initial models (H167A, S216G, N150G, P252A) to generate a mutant protein–substrate complex model for each substrate. Fifty independent energy-minimized structures of the *G462D Ec*LeuA and *H97A/S139G/ N167G/P169A/G462D Ec*LeuA mutant protein–substrate complexes were then calculated. Ligand translational movement and protein side chain torsional movement were allowed during this phase. The top 20 models with the lowest computed ligand energies were used as seeds for final optimization of protein packing and stability with protein backbone coordinates kept fixed. Four final models were calculated from each seed model with force constants (300 and 100 for distance and angle restraints, respectively) applied to the substrates to maintain their position with respect to the residues involved in coordination of the metal ion and the substrate. The best model was selected on the basis of the calculated ligand-binding score and energy score, with a more negative energy score and smaller ligand-binding score denoting a more stable complex. Protein–substrate models are presented in Supporting Information. Solvent-accessible surface area (SASA) values for each atom of each substrate were calculated by RosettaDesign. These atomic SASA values were then added together to determine the SASA of each substrate.

Enzyme Active Site and Substrate Volume Calculations

Models of the *Ec*LeuA mutants were generated on the basis of the 1SR9 PDB structure, which was defined as *G462D Ec*LeuA. PyMol was used to mutate the active site residues (His167, Ser216, Asn150, Pro252) to their backbone-dependent rotamers. Only a single rotamer was available for each mutated residue, removing any ambiguity in side-chain orientation. *G462D* and additional mutant models were analyzed using the Computed Atlas of Surface Topography of proteins (CASTp)[19] server (http://sts.bioengr.uic.edu/castp/ index.php) to determine the approximate solvent-accessible volume of the active site in each model. A probe radius of 1.4 Å was used for these calculations. Substrate van der Waals molecular volumes were calculated using chemicalize.org (http://www.chemicalize.org, accessed August, 2011) by ChemAxon (http://www.chemaxon.com).

Supplementary Material

Refer to Web version on PubMed Central for supplementary material.

Acknowledgments

REFERENCES

1. Atsumi S, Hanai T, Liao JC. Non-fermentative pathways for synthesis of branched-chain higher alcohols as biofuels. Nature. 2008; 451:86–89. [PubMed: 18172501]

2. Steen EJ, Kang Y, Bokinsky G, Hu Z, Schirmer A, McClure A, Del Cardayre SB, Keasling JD. Microbial production of fatty-acid-derived fuels and chemicals from plant biomass. Nature. 2010; 463:559–562. [PubMed: 20111002]

3. Schirmer A, Rude MA, Li X, Popova E, del Cardayre SB. Microbial biosynthesis of alkanes. Science. 2010; 329:559–562. [PubMed: 20671186]

4. Stephanopoulos G. Challenges in engineering microbes for biofuels production. Science. 2007; 315:801–804. [PubMed: 17289987]

5. Causey TB, Zhou S, Shanmugam KT, Ingram LO. Engineering the metabolism of Escherichia coli W3110 for the conversion of sugar to redox-neutral and oxidized products: homoacetate production. Proc. Natl. Acad. Sci. U.S.A. 2003; 100:825–832. [PubMed: 12556564]

6. Lin H, Bennett GN, San KY. Metabolic engineering of aerobic succinate production systems in Escherichia coli to improve process productivity and achieve the maximum theoretical succinate yield. Metab. Eng. 2005; 7:116–127. [PubMed: 15781420]

7. Zha W, Shao Z, Frost JW, Zhao H. Rational pathway engineering of type I fatty acid synthase allows the biosynthesis of triacetic acid lactone from d-glucose in vivo. J. Am. Chem. Soc. 2004; 126:4534–4535. [PubMed: 15070368]

8. Cane DE, Walsh CT, Khosla C. Harnessing the biosynthetic code: combinations, permutations, and mutations. Science. 1998; 282:63–68. [PubMed: 9756477]

9. McCoy M, Reisch MS, Tullo AH, Tremblay JF, Voith M. Output declines in U.S., Europe. Chem. Eng. News. 2010; 88:54–62.

10. Zhang K, Sawaya MR, Eisenberg DS, Liao JC. Expanding metabolism for biosynthesis of nonnatural alcohols. Proc. Natl. Acad. Sci. U.S.A. 2008; 105:20653–20658. [PubMed: 19064911]

11. Berg, JM.; Tymoczko, JL.; Stryer, L. Biochemistry. 5th ed.. W. H. Freeman; New York: 2002.

12. Stieglitz BI, Calvo JM. Distribution of the isopropylmalate pathway to leucine among diverse bacteria. J. Bacteriol. 1974; 118:935–941. [PubMed: 4829932]

13. Cole FE, Kalyanpur MG, Stevens CM. Absolute configuration of alpha isopropylmalate and the mechanism of its conversion to beta isopropylmalate in the biosynthesis of leucine. Biochemistry. 1973; 12:3346–3350. [PubMed: 4270046]

14. Burns RO, Umbarger HE, Gross SR. The biosynthesis of leucine. III. The conversion of alpha-hydroxy-beta-carboxyisocaproate to alpha-ketoisocaproate. Biochemistry. 1963; 2:1053–1058. [PubMed: 14087358]

15. Chérest M, Felkin H, Prudent N. Torsional strain involving partial bonds. The stereochemistry of the lithium aluminium hydride reduction of some simple open-chain ketones. Tetrahedron Lett. 1968; 9:2199–2204.

16. Anh NT, Eisenstein O, Lefour JM, Dau METH. Orbital factors and asymmetric induction. J. Am. Chem. Soc. 1973; 95:6146–6147.

17. Koon N, Squire CJ, Baker EN. Crystal structure of LeuA from Mycobacterium tuberculosis, a key enzyme in leucine biosynthesis. Proc. Natl. Acad. Sci. U.S.A. 2004; 101:8295–8300. [PubMed: 15159544]

18. Gusyatiner, MM.; Lunts, MG.; Kozlov, YI.; Ivanovskaya, LV.; Voroshilova, EB. Anjinomoto Co., Inc.; Tokyo: 2002. DNA coding for mutant isopropylmalate synthase L-leucine-producing microorganism and method for producing L-leucine. U.S. Patent 6403342

19. Dundas J, Ouyang Z, Tseng J, Binkowski A, Turpaz Y, Liang J. CASTp: computed atlas of surface topography of proteins with structural and topographical mapping of functionally annotated residues. Nucleic Acids Res. 2006; 34:W116–118. [PubMed: 16844972]

20. Kuhlman B, Baker D. Native protein sequences are close to optimal for their structures. Proc. Natl. Acad. Sci. U.S.A. 2000; 97:10383–10388. [PubMed: 10984534]

21. Larroy C, Rosario Fernandez M, Gonzalez E, Pares X, Biosca JA. Properties and functional significance of Saccharomyces cerevisiae ADHVI. Chem.-Biol. Interact. 2003; 143–144:229–238.

22. Zhang K, Li H, Cho KM, Liao JC. Expanding metabolism for total biosynthesis of the nonnatural amino acid l-homoalanine. Proc. Natl. Acad. Sci. U.S.A. 2010; 107:6234–6239. [PubMed: 20332210]

23. Shen CR, Liao JC. Metabolic engineering of Escherichia coli for 1-butanol and 1-propanol production via the ketoacid pathways. Metab. Eng. 2008; 10:312–320. [PubMed: 18775501]

24. Ehrlich F. Concerning the conditions for fusel oil formation and concerning its connection with the protein formation of yeast. Ber. Dtsch. Chem. Ges. 1907; 40:1027–1047.

25. Dekishima Y, Lan EI, Shen CR, Cho KM, Liao JC. Extending carbon chain length of 1-butanol pathway for 1-hexanol synthesis from glucose by engineering Escherichia coli. J. Am. Chem. Soc. 2011; 133:11399–11401. [PubMed: 21707101]

26. Dellomonaco C, Clomburg JM, Miller EN, Gonzalez R. Engineered reversal of the β-oxidation cycle for the synthesis of fuels and chemicals. Nature. 2011; 476:355–359. [PubMed: 21832992]

27. Drevland RM, Waheed A, Graham DE. Enzymology and evolution of the pyruvate pathway to 2-oxobutyrate in Methanocaldococcus jannaschii. J. Bacteriol. 2007; 189:4391–4400. [PubMed: 17449626]

28. Altschul SF, Madden TL, Schaffer AA, Zhang J, Zhang Z, Miller W, Lipman DJ. Gapped BLAST and PSI-BLAST: a new generation of protein database search programs. Nucleic Acids Res. 1997; 25:3389–3402. [PubMed: 9254694]

29. Wallon G, Yamamoto K, Kirino H, Yamagishi A, Lovett ST, Petsko GA, Oshima T. Purification, catalytic properties and thermostability of 3-isopropylmalate dehydrogenase from Escherichia coli. Biochim. Biophys. Acta. 1997; 1337:105–112. [PubMed: 9003442]

30. Wallon G, Kryger G, Lovett ST, Oshima T, Ringe D, Petsko GA. Crystal structures of Escherichia coli and Salmonella typhimurium 3-isopropylmalate dehydrogenase and comparison with their thermophilic counterpart from Thermus thermophilus. J. Mol. Biol. 1997; 266:1016–1031. [PubMed: 9086278]

31. Miyazaki K, Kakinuma K, Terasawa H, Oshima T. Kinetic analysis on the substrate specificity of 3-isopropylmalate dehydrogenase. FEBS Lett. 1993; 332:35–36. [PubMed: 8405445]

32. de la Plaza M, Fernandez de Palencia P, Pelaez C, Requena T. Biochemical and molecular characterization of alpha-ketoisovalerate decarboxylase, an enzyme involved in the formation of aldehydes from amino acids by Lactococcus lactis. FEMS Microbiol Lett. 2004; 238:367–374. [PubMed: 15358422]

33. Larroy C, Fernandez MR, Gonzalez E, Pares X, Biosca JA. Characterization of the Saccharomyces cerevisiae YMR318C (ADH6) gene product as a broad specificity NADPH-dependent alcohol dehydrogenase: relevance in aldehyde reduction. Biochem. J. 2002; 361:163–172. [PubMed: 11742541]

34. Kellogg BA, Poulter CD. Chain elongation in the isoprenoid biosynthetic pathway. Curr. Opin. Chem. Biol. 1997; 1:570–578. [PubMed: 9667899]

35. Carreras CW, Pieper R, Khosla C. The chemistry and biology of fatty acid, polyketide, and nonribosomal peptide biosynthesis. Top. Curr. Chem. 1997; 188:85–126.

36. Lutz R, Bujard H. Independent and tight regulation of transcriptional units in Escherichia coli via the LacR/O, the TetR/O and AraC/I1-I2 regulatory elements. Nucleic Acids Res. 1997; 25:1203–1210. [PubMed: 9092630]

37. Frisch, MJ.; Trucks, GW.; Schlegel, HB.; Scuseria, GE.; Robb, MA.; Cheeseman, JR.; Scalmani, G.; Barone, V.; Mennucci, B.; Petersson, GA.; Nakatsuji, H.; Caricato, M.; Li, X.; Hratchian, HP.; Izmaylov, AF.; Bloino, J.; Zheng, G.; Sonnenberg, JL.; Hada, M.; Ehara, M.; Toyota, K.; Fukuda, R.; Hasegawa, J.; Ishida, M.; Nakajima, T.; Honda, Y.; Kitao, O.; Nakai, H.; Vreven, T.; Montgomery, JA.; Peralta, JE.; Ogliaro, F.; Bearpark, M.; Heyd, JJ.; Brothers, E.; Kudin, KN.; Staroverov, VN.; Kobayashi, R.; Normand, J.; Raghavachari, K.; Rendell, A.; Burant, JC.; Iyengar, SS.; Tomasi, J.; Cossi, M.; Rega, N.; Millam, JM.; Klene, M.; Knox, JE.; Cross, JB.; Bakken, V.; Adamo, C.; Jaramillo, J.; Gomperts, R.; Stratmann, RE.; Yazyev, O.; Austin, AJ.; Cammi, R.; Pomelli, C.; Ochterski, JW.; Martin, RL.; Morokuma, K.; Zakrzewski, VG.; Voth, GA.; Salvador, P.; Dannenberg, JJ.; Dapprich, S.; Daniels, AD.; Farkas; Foresman, JB.; Ortiz, JV.; Cioslowski, J.; Fox, DJ. Gaussian 09, Revision A.02. Gaussian, Inc.; Wallingford, CT: 2009.

38. Schutz CN, Warshel A. What are the dielectric "constants" of proteins and how to validate electrostatic models? Proteins. 2001; 44:400–417. [PubMed: 11484218]

39. Simonson T, Brooks CL. Charge screening and the dielectric constant of proteins: Insights from molecular dynamics. J. Am. Chem. Soc. 1996; 118:8452–8458.

40. van der Kamp MW, Perruccio F, Mulholland AJ. Ab initio QM/MM modelling of acetyl-CoA deprotonation in the enzyme citrate synthase. J. Mol. Graph. Model. 2007; 26:676–690. [PubMed: 17493853]
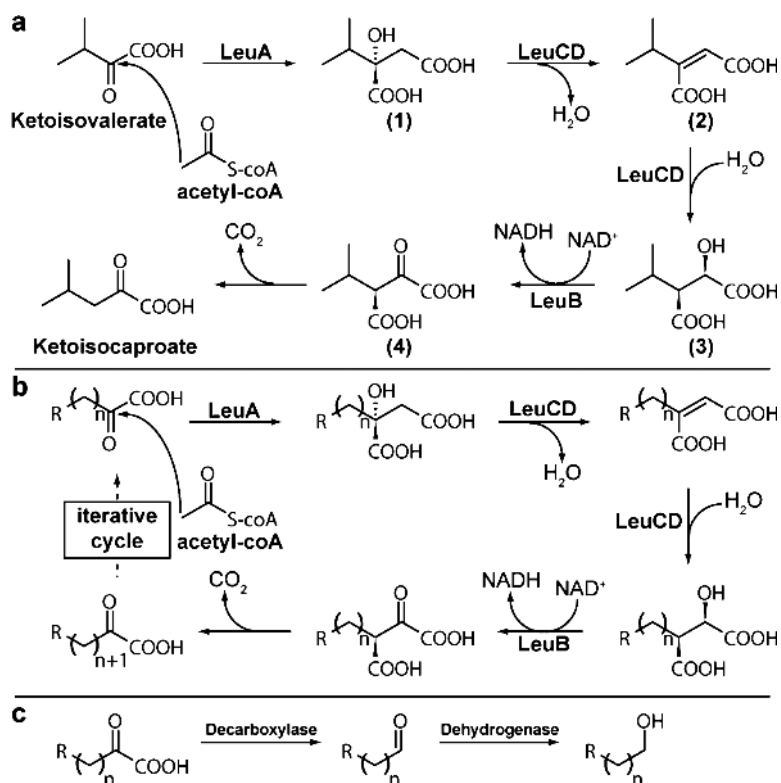
Figure 1.
Engineering *Ec*LeuABCD "+1" biosynthetic pathway. (a) Reaction mechanism of the LeuABCD pathway. Natural substrate ketoisovalerate is converted to ketoisocaproate after five enzyme-catalyzed chemical steps. (b) Theoretical "+1" recursive elongation of 2-ketoacid substrates containing different R-groups. This pathway enables the biosynthesis of nonnatural ketoacids. (c) Alcohols are produced from 2-ketoacids by enzymatic decarboxylation and reduction.
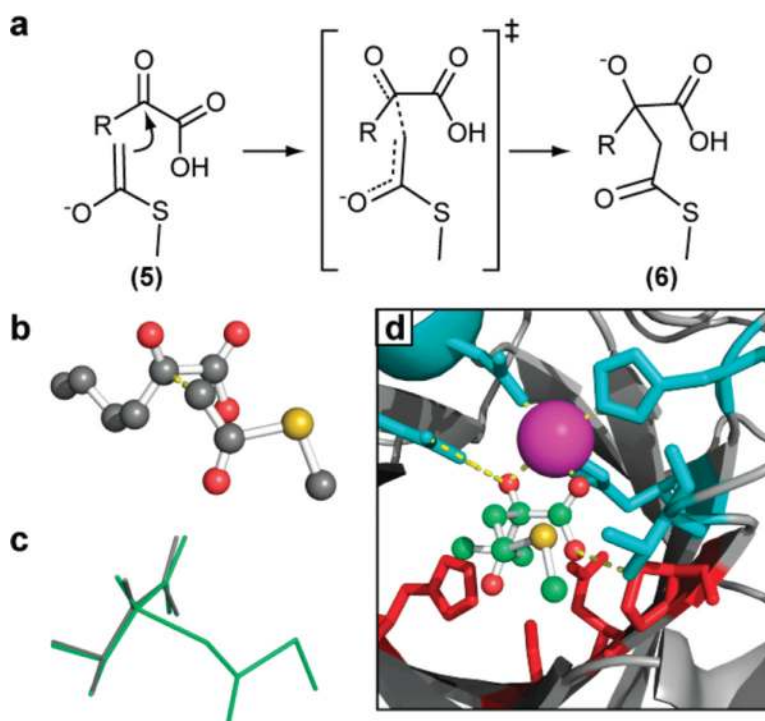
Figure 2.
Modeling of carbon–carbon bond formation and the *Ec*LeuA active site. (a) Quantum mechanical model of the carbon–carbon bond formation step catalyzed by LeuA. A 2-ketoacid is attacked by 1-(methylthio)ethenolate (**5**) (a model for acetyl-CoA), resulting in the formation of a 2-ketoacid enolate (**6**). (b) View of 2-ketocaproate and 1-(methylthio)ethenolate oriented in the pretransition state, as determined by QM calculations with Gaussian09.[37] The 4-carbon alkyl R-group of 2-ketocaproate is oriented away from the incoming 1-(methylthio)ethenolate nucleophile. (c) View of ketoisovalerate from PDB 1SR9 (gray) and the ketoisovalerate enolate calculated by QM (green) aligned over 8 shared heavy atoms (rmsd = 0.15 Å). (d) *Ec*LeuA active site modeled with ketoisovalerate enolate. Residues involved in coordinating the Zn^{2+} metal ion (magenta sphere) and the substrate (green, red, and yellow ball-and-stick) are shown in cyan (Arg12, Asp14, Thr171, His202, His204 in *Ec*LeuA; corresponding to Arg80, Asp81, Thr254, His285, His287 in *Mt*LeuA.[17] Coordination interactions are shown as dashed yellow lines. Residues within 4.5 Å of the γ-methyl of ketoisovalerate (other than those involved in metal ion and substrate coordination) are shown in red. The protein backbone is shown as a gray cartoon.
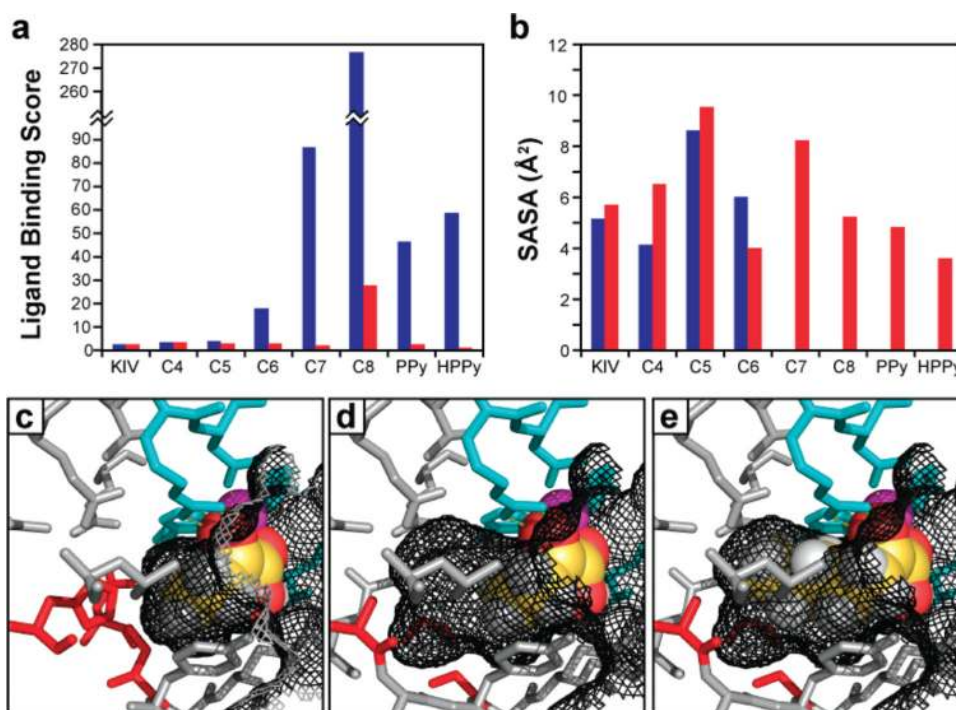
Figure 3.
Comparison of substrate binding and substrate solvent-accessible surface area in feedback-resistant and quintuple mutant *Ec*LeuA protein–substrate complex models. (a) Ligand-binding score of substrates, as calculated by Rosetta. Smaller scores indicate lower calculated energy parameters and better substrate binding. Scores for substrates in complex with the *G462D* and *H97A*/*S139G*/*N167G*/*P169A*/*G462D* mutant proteins are shown in blue and red, respectively. (b) Solvent-accessible surface area (SASA) of substrates in the binding pockets of *G462D* (blue) and *H97A*/*S139G*/*N167G*/*P169A*/*G462D* mutant (red) proteins, as calculated by RosettaDesign. SASA values for C7, C8, PPy, and HPPy in the *G462D* protein binding pocket have no meaning due to the steric clash observed between these substrates and the enzyme (Supplementary Figure S1) and are therefore not shown. (c–e) Protein–substrate models with binding pockets shown as wire mesh and substrates shown as spheres. Protein residues, metal ion, and coordination interactions are shown and colored as indicated in Figure 2. (c) *G462D* protein with C4 substrate. (d) *H97A*/*S139G*/*N167G*/*P169A*/*G462D* mutant protein with C4 substrate. (e) *H97A*/*S139G*/*N167G*/*P169A*/*G462D* mutant protein with C7 substrate.
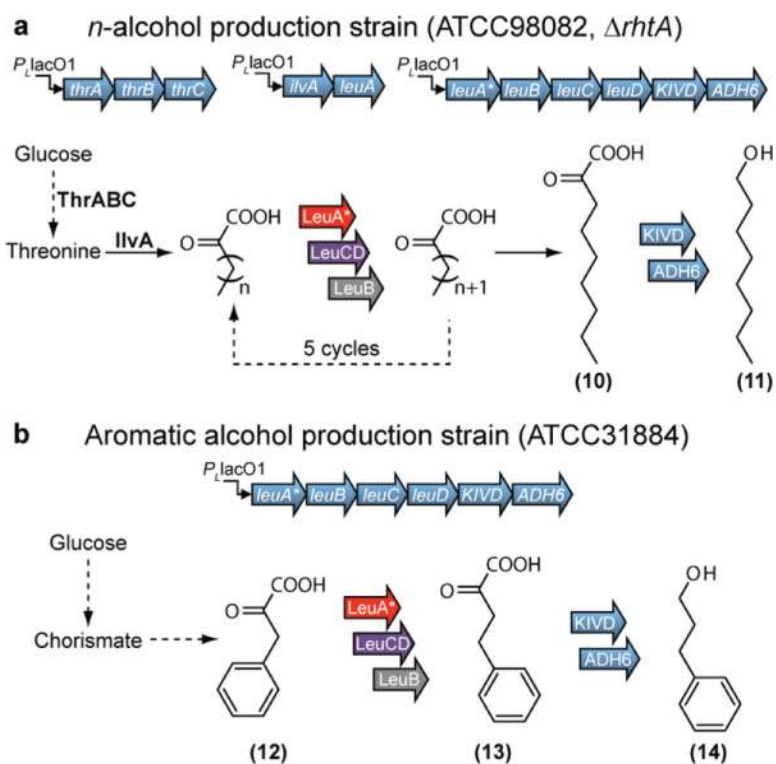
Figure 4.
Metabolic engineering of *E. coli* for long-chain alcohol production. (a) Synthetic operons for gene expression in threonine overproducer to produce linear chain alcohols. Overexpression of ThrABC and IlvA drives the carbon flux toward 2-ketobutyrate. Engineered protein *H97A|S139G|N167G|P169A|G462D Ec*LeuA (LeuA*) enables *Ec*LeuA*BCD to catalyze recursive elongation of natural metabolite 2-ketobutyrate ($n = 1$) to 2-ketooctanoate (**10**). Decarboxylation and reduction of 2-ketononanoate by Kivd and Adh6 results in 1-octanol (**11**). (b) Synthetic operons for gene expression in phenylalanine overproducer. LeuA* enables the elongation of phenylpyruvate (**12**) into homophenylpyruvate (**13**). Decarboxylation and reduction of 2-ketononanoate by Kivd and Adh6 result in phenylpropanol (**14**).

Table 1

Quantum Mechanical Calculation Results

substrate	$\Delta G^{\ddagger}$ (kcal/mol)	$\Delta G_{reaction}$ (kcal/mol)	transition state distance (Å)[a]
ketoisovalerate	9.1	9.0	2.03
2-ketobutryate	9.3	7.4	2.05
2-ketovalerate	9.2	8.6	2.04
2-ketocaproate	9.4	8.8	2.04
2-ketoheptanoate	9.2	8.2	2.04
2-ketooctanoate	9.0	8.6	2.04
phenylpyruvate	6.4	6.4	2.12
homophenylpyruvate	7.5	7.5	1.98

[a] Distance between the a carboxyl carbon of the 2-keto acid and the nucleophilic carbon of the acetyl-CoA analogue 1-(methylthio)-ethenolate.

Table 2

Enzyme Binding Pocket and Substrate Volumes

enzyme mutation(s)	increase in solvent-accessible vol (Å³)[b]	substrate	increase in molecular vol (Å³)[c]
G462D[a]	0	2-ketobutyrate	0
S139G, G462D	5.1	2-ketovalerate	17.0
S139G, N167A, G462D	9.2	ketoisovalerate	17.2
H97A, S139G, G462D	33.4	2-ketocaproate	34.0
H97A, S139G, N167A, G462D	42.6	2-ketoheptanoate	50.9
H97A, S139G, N167G, G462D	47.0	phenylpyruvate	53.7
H97A, S139G, N167G, P169A, G462D	50.0	2-ketoocatanoate	67.8
		homophenylpyruvate	70.6

[a]The feedback-resistant *Ec*LeuA mutant.

[b]Relative to a solvent-accessible volume for *G462D Ec*LeuA of 60.0 Å³, as calculated by CASTp[19] (http://sts.bioengr.uic.edu/castp/index.php).

[c]Relative to a molecular volume for 2-Ketobutyrate of 92.1 Å³, as calculated by chemicalize.org (http://www.chemicalize.org).

Table 3

Kinetic Parameters of Feedback-Resistant and Quintuple Mutant *Ec*LeuA

substrate	G462D *Ec*LeuA[a]			*Ec*LeuA H97A, S139G, N167G, P169A, G462D mutant		
	K_m (μM)	k_{cat} (s⁻¹)	k_{cat}/K_m (mM⁻¹ s⁻¹)	K_m (μM)	k_{cat} (s⁻¹)	k_{cat}/K_m (mM⁻¹ s⁻¹)
ketoisovalerate (KIV)	206 ± 21[b]	1.15 ± 0.03	5.58 ± 0.59	583 ± 68	0.96 ± 0.04	1.65 ± 0.20
2-ketobutyrate (C4)	345 ± 21	2.43 ± 0.04	7.04 ± 0.44	657 ± 31	3.27 ± 0.05	4.98 ± 0.25
2-ketovalerate (C5)	135 ± 10	0.73 ± 0.012	5.41 ± 0.41	815 ± 63	4.52 ± 0.13	5.54 ± 0.46
2-ketocaproate (C6)	105 ± 10	0.026 ± 0.001	0.25 ± 0.03	456 ± 86	6.51 ± 0.39	14.28 ± 2.83
2-ketoheptanoate (C7)	0	0	0	349 ± 80	5.21 ± 0.35	14.93 ± 3.57
2-ketooctanoate (C8)	0	0	0	455 ± 69	3.49 ± 0.17	7.67 ± 1.22
phenylpyruvate	0	0	0	118 ± 26	0.09 ± 0.01	0.77 ± 0.18
homophenylpyruvate	0	0	0	575 ± 101	0.38 ± 0.02	0.66 ± 0.12

[a]The feedback-resistant *Ec*LeuA mutant.

[b]All values represent the average of three independent experiments, with standard deviation indicated.

NIH-PA Author Manuscript

NIH-PA Author Manuscript

NIH-PA Author Manuscript

Table 4

Alcohol Production Profiles of *Ec*LeuA mutants

enzyme mutation(s)	additional *Ec*LeuA G462D[a]	*n*-alcohols produced (mg L^{-1})						
		1-propanol	1-butanol	1-pentanol	1-hexanol	1-heptanol	1-octanol
G462D[a]	+	35 ± 10[b]	58 ± 1	953 ± 39	31 ± 3	ND[c]	ND
S139G, G462D	+	316 ± 78	993 ± 181	2220 ± 142	219 ± 11	4.8 ± 1.4	ND
S139G, N167A, G462D	+	303 ± 145	843 ± 223	1380 ± 69	204 ± 13	8.9 ± 1.7	ND
H97A, S139G, G462D	+	285 ± 34	872 ± 71	1751 ± 120	302 ± 33	24 ± 3.9	ND
H97A, S139G, N167A, G462D	+	329 ± 38	897 ± 81	957 ± 42	148 ± 6.5	77 ± 9.8	ND
H97A, S139G, N167G, G462D	+	368 ± 15	932 ± 79	1131 ± 107	104 ± 11	41 ± 9.9	ND
H97A, S139G, N167G, P169A, G462D	+	105 ± 20	406 ± 47	656 ± 50	146 ± 10	80 ± 11	2.0 ± 0.26
H97A, S139G, N167G, P169A, G462D	–	187 ± 37	374 ± 38	148 ± 8	109 ± 12	23 ± 4	ND

[a]The feedback-resistant *Ec*LeuA mutant.

[b]All values represent the average of three independent experiments, with standard deviation indicated.

[c]ND = not detected.